Current Biology *17*, 694–699, April 17, 2007 ©2007 Elsevier Ltd All rights reserved DOI 10.1016/j.cub.2007.02.058

Report

The Universal Dynamics of Cell Spreading

Damien Cuvelier,[1,4] Manuel Théry,[2,6] Yeh-Shiu Chu,[3,7] Sylvie Dufour,[3] Jean-Paul Thiéry,[3,7] Michel Bornens,[2] Pierre Nassoy,[1,*] and L. Mahadevan[4,5,*]

[1] Physical Chemistry "Curie"
UMR 168
[2] Biology of Cell Cycle and Cell Motility
[3] Cellular Morphogenesis and Tumor Progression
UMR 144
Institut Curie
75005 Paris
France
[4] Division of Engineering and Applied Sciences
Harvard University
Cambridge, Massachusetts 02138
[5] Department of Systems Biology
Harvard Medical School
Boston, Massachusetts 02115
[6] Institute of Life Sciences Research and Technologies
Laboratoire Biopuces
Commissariat à l'Energie Atomique
38054 Grenoble
France
[7] Institute of Molecular and Cell Biology
Proteos 6-03
138673 Singapore

Summary

Cell adhesion and motility depend strongly on the interactions between cells and extracellular matrix (ECM) substrates. When plated onto artificial adhesive surfaces, cells first flatten and deform extensively as they spread. At the molecular level, the interaction of membrane-based integrins with the ECM has been shown to initiate a complex cascade of signaling events [1], which subsequently triggers cellular morphological changes and results in the generation of contractile forces [2]. Here, we focus on the early stages of cell spreading and probe their dynamics by quantitative visualization and biochemical manipulation with a variety of cell types and adhesive surfaces, adhesion receptors, and cytoskeleton-altering drugs. We find that the dynamics of adhesion follows a universal power-law behavior. This is in sharp contrast with the common belief that spreading is regulated by either the diffusion of adhesion receptors toward the growing adhesive patch [3–5] or by actin polymerization [6–8]. To explain this, we propose a simple quantitative and predictive theory that models cells as viscous adhesive cortical shells enclosing a less viscous interior. Thus, although cell spreading is driven by well-identified biomolecular interactions, it is dynamically limited by its mesoscopic structure and material properties.

*Correspondence: pierre.nassoy@curie.fr (P.N.), lm@deas.harvard.edu (L.M.)

Results

We address the dynamics of cell spreading after contact initiation and preceding cell polarization. To do this, we quantitatively monitored the spreading dynamics of individual cells by using reflection interference contrast microscopy (RICM), which enabled us to visualize the adhesive contact between the cell membrane and surface [9], over a period of up to an hour in a serum-free medium. In most cases, the growth of the adhesion patch was found to be isotropic (Figure 1 and Movie S1 in the Supplemental Data available online), consistent with previous findings [10], and allowed us to define an average contact radius, $R = \sqrt{A/\pi}$ (with "A" being the contact area measured from image analysis) as a function of different surface coatings, several cell lines (wild-type or mutant), and various cytoskeleton-altering drugs.

When the surface was coated with a typical ECM protein, fibronectin, we found that the extent of spreading of different cell types such as HeLa and sarcoma murine (S180) cells was correlated with the fibronectin surface density (Figure S1). However, in the early stages, the growth rate of the contact radius obtained by subtraction of the lag time for spreading initiation was unaffected by fibronectin surface density (Figure S1). This observation is similar to that previously reported for the spreading of fibroblasts [10]. To understand the effect of other adhesion proteins, we used S180 cells expressing E-cadherin, a homophilic cell-cell adhesion protein [11], on E-cadherin-decorated surfaces (Movie S2). Quite surprisingly, this too left the overall dynamical behavior invariant during the time course of the experiment (Figure 2, green triangles).

When S180 cells were transiently transfected with a vector encoding for the constitutively inactive construct of Cdc42, again there was no significant change in the early stages of spreading (Figure 2, red circles, and Movie S3). Because filopodia are inhibited by Cdc42DN [12], these experiments demonstrate that the cell membrane "roughness" induced by filopodia is not a major determinant in driving the initial stages of spreading.

To further assess the hypothesized role of the diffusion of adhesion receptors [3–5], we carried out similar experiments by using polylysine-coated slides. In this case, cell attachment was nonspecific, and although the lag time for spreading initiation was reduced, the dynamical behavior of the contact radius was again found to be identical to the previous results (Figure 2, blue triangles, and Movie S6).

Moving from the manipulation of surface proteins and external features, we next investigated the role of the cytoskeletal network of microtubules by seeding nocodazol-treated HeLa cells on fibronectin-coated surfaces. Although cell spreading was not impaired by microtubule-disrupting agents, the absence of microtubule-disrupting agents leads to the formation of localized

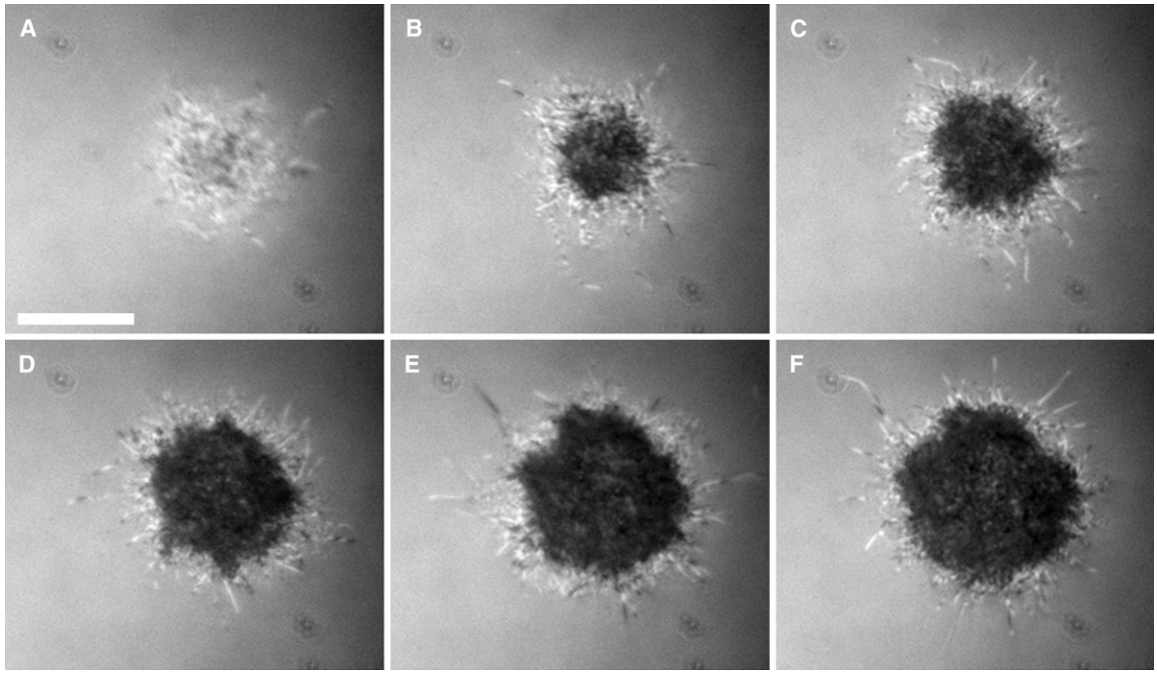

Figure 1. Reflection Interference Contrast Snapshots of a HeLa Cell Spreading onto a Fibronectin-Coated Glass Substrate

The time interval between successive images (A)–(F) is 150 s. The scale bar represents 5 μm. The growth of the adhesive patch (dark zone) is isotropic. Filopodia are visible as bright-dark dotted hairs at the periphery of the cell.

cellular blebs [13] (Movies S4 and S5). This led to fluctuations in the size of the contact radius. However, overall the growth of the average patch size remained similar to the one found for intact cells (Figure 2, purple squares).

The independence of the temporal evolution of the contact radius on the surface properties of both the cell and the substrate, on the cell type, and on certain cytoskeletal altering drugs suggests that although the growth of the adhesive patch may be regulated by the complex signaling events upstream of its formation, it is ultimately limited by some collective aspects of the cell's material behavior, such as its geometry and thermodynamic and mechanical properties. In Figure 2, we show that quantifying the temporal evolution of adhesive contact for all the cases above shows two universal trends; the contact radius follows an initial diffusive regime summarized by the scaling law $R \sim t^{1/2}$ initially before it slows down to a subdiffusive behavior summarized by the scaling law $R \sim t^{1/4}$.

To explain these growth laws, we propose a theoretical model on the basis of a simplified physicochemical description of the cell. On the time scale of the experiments, we model the cell with its actin cortex as

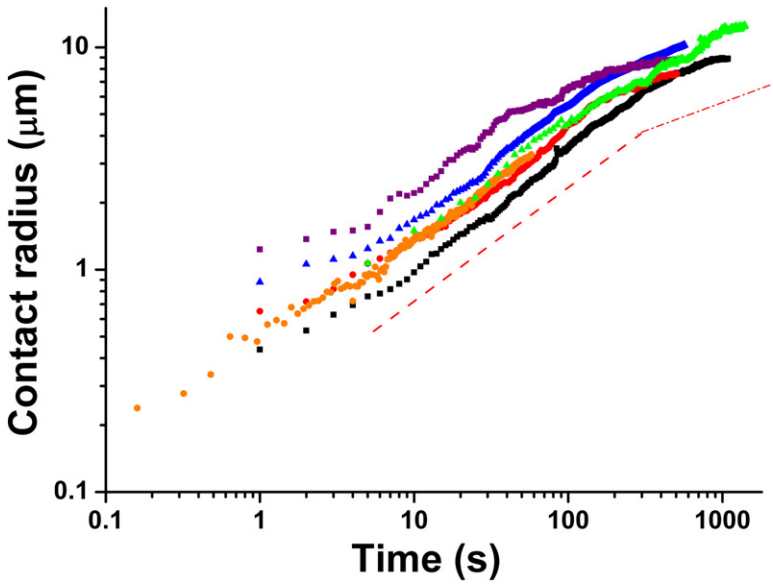

Figure 2. Growth of Cell-Substrate Adhesive Patches during the Early Stages of Spreading Exhibits a Universal Power Law that Is Independent of Cell Type, Substrate, and Adhesion Receptors

Time corresponds to that after the onset of spreading, i.e., lag times are subtracted. The average contact radius, based on contact-area measurements (see text) increases initially as $t^{1/2}$(the red dashed line indicates $R \sim t^{1/2}$) over more than three decades in time before slowing down (the red dash-dotted line indicates $R \sim t^{1/4}$) (see Equations 1 and 2). The different curves are representative of a variety of experimental conditions corresponding to: (black square) HeLa cell/fibronectin (1 μg/ml) substrate; (green triangle) E-cadherin S180 cell/E-cadherin substrate; (red circle) Cdc42DN S180 cell/fibronectin substrate; (purple square) nocodazol-treated HeLa cell/fibronectin substrate; (blue triangle) HeLa cell/polylysine substrate; and (orange circle) biotinylated red blood cell/streptavidin substrate.

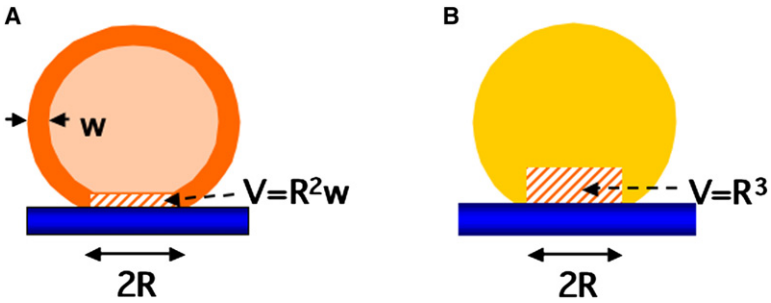

Figure 3. Schematic Representation of the Cell

(A) As a viscous shell enclosing a liquid for intact cells. The volume in which viscous dissipation occurs is shaded.

(B) As a homogeneous viscous drop for cells without cortex (i.e., treated with cytochalasin D). The volume in which viscous dissipation occurs is shaded.

a membrane-bound viscous shell that encloses a liquid cytoplasm (Figure 3). During spreading, the increase in cell contact with the surface is driven by the adhesion associated with the formation of both specific bonds and nonspecific interactions. Concomitantly, spreading causes cell deformation and flattening, which leads to a dissipation of energy. The dynamical balance between these processes determines the temporal evolution of adhesive contact. Of course, the cell itself is a source of energy that can be and is used for remodeling its structure. Here, we explicitly assume that during the early stages of adhesion, this energy is not directed explicitly at enhancing or reducing adhesion, although clearly this is not true during active actin polymerization in the later stages of spreading when lamellipodia are formed.

Then, for a rate of change of the contact area $\frac{dA}{dt} \approx R\frac{dR}{dt}$ (assuming a disk-like shape for the contact zone), the rate of energy gain is $JR\frac{dR}{dt}$, where J the adhesion energy per unit area is the product of the areal density of adhesive bonds and the energy per bond. To accommodate adhesion, the viscous cortical shell has to flatten and flow during spreading. At short times, the size of the contact zone is comparable to the length of cortical filaments, so that the velocity induced in the cortical shell by its unbending in the vicinity of the contact line must be accommodated by the shearing of filaments over the entire contact zone. Because the lower part of the cortex is attached to the substrate, this physical picture implies a characteristic strain rate of order $\frac{dR/dt}{w}$. We note that this picture is very different from that of a drop made of a simple (Newtonian) liquid such as water, where the strain rate is localized to a zone of size comparable to the contact radius. Because flow in the thin dense cortex dominates that in the rest of the cytoplasm, the characteristic volume over which dissipation occurs is of order R^2w (see Theoretical Model under the Supplemental Discussion for details). If η is the cortical-shell viscosity, the energy dissipation rate due to the viscous flow in the cortical shell is proportional to $\eta(\frac{dR}{dt}\frac{1}{w})^2R^2w$. Balancing this with the adhesive power leads to following scaling law for the contact radius at short times

$$R = C\left(\frac{Jw}{\eta}\right)^{1/2} \cdot t^{1/2},\ R \le R_c, \qquad (1)$$

with C being a dimensionless constant and R_c being the initial radius of the cell.

In this model, a key assumption is that the cortical actin behaves as a polymeric viscous shell. Although cells generally exhibit an overall complex viscoelastic mechanical behavior, Käs and coworkers [14] have shown that cells can be characterized by an effective viscosity at deforming frequencies lower than ~0.1Hz (or characteristic deforming times greater than ~10 s). Because the spreading of cells of 10 μm size typically occurs within tens of minutes, this sets the average shear rate at approximately 10^{-4} Hz, which is well in the range of viscous response. The power law obtained from Equation 1 is in good agreement with experimental data over nearly four decades in time, as seen in the representative curves of Figure 2. As expected, the scaling laws predict that higher adhesion energies yield larger patch sizes for a given time; thus, the R versus t curves are shifted upward and to the right when, for instance, the concentration in fibronectin on the substrate is increased. By using measured values for the various parameters [15, 16] (w = 1 μm, η = 300 Pa.s, and J = 40 μJ/m^2 for fibronectin coating at 1 μg/ml), we find that with $C \sim 0.8–2.5$, Equation 1 provides an excellent quantitative description of all our experimental results (see Table S1, which summarizes the parameter values for all the situations that we have experimentally investigated—with data from approximately 10 cells for each different condition).

At longer times, the radius of the adhesive patch is comparable to the cell size, so that viscous dissipation occurs in the whole cell, which is substantially flattened at this stage. If w_c is the height of the cell of initial radius R_c, it follows that $R_c^3 \sim R^2w_c$ because of volume conservation. Then, the balance between the adhesive and viscous power is modified to $JR\frac{dR}{dt} \cong \eta_c(\frac{dR}{dt}\frac{1}{w_c})^2R^2w_c$ and leads to the scaling law as follows:

$$R \sim \left(\frac{JR_c^3}{\eta_c}\right)^{1/4} t^{1/4},\ R > R_c \qquad (2)$$

with η_c being the effective cell viscosity, which is in principle different from the cortical viscosity. This second regime, corresponding to a slowing down of the growth of the adhesive patch, is also qualitatively consistent with our experimental results, although the temporal range over which we were able to test this is limited. This intermediate stage of cell spreading corresponds to a transient state between the initial cell flattening that is our main focus here and the active cell remodeling associated with such events as lamellipodium protrusions and thus may be blurred. In contrast, the first regime, characterized by a linear increase of the contact area with time, is a very robust feature of cell spreading.

The temporal evolution of cell spreading described by our simple model predicts a dependence on parameters such as the geometry and rheological properties of the cortical shell and the adhesion energy per unit area of

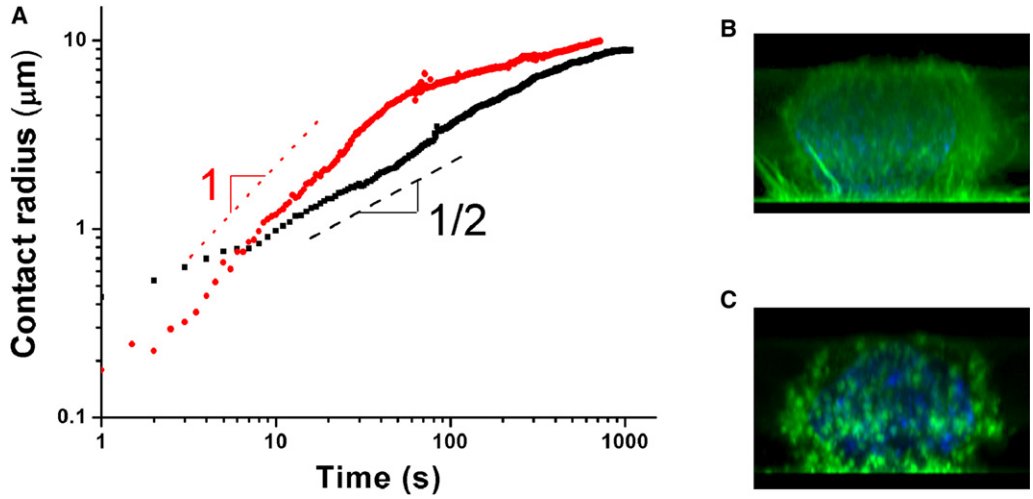

Figure 4. Disruption of the Cortical Actin Significantly Affects the Spreading Dynamics

(A) In contrast with untreated HeLa cells (black squares), cytochalasin D-treated cells (red circles) spread more quickly and further as characterized by a linear increase of the average contact radius with time. The surface is coated with fibronectin. The various lines indicate the different power laws based on our simple theory (see text). (B) Three-dimensional multicolor image of an untreated HeLa cell on a fibronectin-coated substrate 30 min after spreading initiation. Nucleus (shown in blue) is hardly visible behind a dense actin cortex (shown in green). Vinculin labeling was undetectable, suggesting that focal adhesions are not formed at this stage of spreading.

(C) Three-dimensional multicolor image of a cytochalasin D-treated cell on a fibronectin-coated substrate 30 min after spreading initiation. The actin cortex is mostly disrupted because actin (shown in green) appears patchy.

the cell to the substrate and is thus falsifiable. In order to critically test our model, we have performed two additional series of experiments.

First, if valid, our description should be applicable to all types of cells. An extreme variant in terms of both geometry and mechanical properties is provided by red blood cells whose cytoskeleton is just a thin spectrin network. Biotinylated red blood cells that have been osmotically swollen to become spherical spread onto streptavidin-coated surfaces completely within 1 min (Movie S7), more than an order-of-magnitude more quickly than eukaryotic cells. Yet the growth law remains unchanged (Figure 2, orange circles) and is consistent with our predictions with the following typical values [17–19]: w= 50 nm, η = 10 Pa.s and J = 100 μJ/m^2, which yield a value $C \sim 2$ for the prefactor in Equation 1. To put our study in a wider comparative context, we searched the literature for previous experimental reports of cell-spreading dynamics. Although most were primarily descriptive or focused on very specific molecular mechanisms, we found that the kinetics of spreading for fibroblasts on fibronectin-coated glass [10], *Dictyostelium discoideum* on bare glass [6], or erythrocytes on polylysine-coated glass [20] fall into the rubric outlined here quantitatively or semiquantitatively (see Quantitative Interpretation in the Supplemental Discussion for detailed analysis).

Second, whereas microtubule disruption had no effect on the spreading dynamics, we expect drastic changes if the actin cortex shell is altered because its geometry and mechanical properties enter directly into our model. On treating HeLa cells with cytochalasin D, we found that the growth of the adhesion zone (Movie S8) was linear in time (Figure 4A) as the cortex became visibly patchy (Figures 4B and 4C). This is qualitatively consistent with the fact that the flow of cortical actin is the rate-limiting step. However, when the cortex is destroyed, the problem of cell spreading becomes somewhat analogous to the spreading of a very viscous drop with dissipation occurring within a contact zone of volume R^3, wherein the power balance at short times reads $JR\frac{dR}{dt} \cong \eta_c(\frac{dR}{dt}\frac{1}{R})^2R^3$, and leads to the scaling law $R \cong (\frac{J}{\eta_c})t$. At longer times, when the cell is flattened so that dissipation is no longer limited to just the contact zone but occurs in the whole cell, we expect a crossover to Equation 2, in fair agreement with our measurements, as seen in Figure 4A.

Discussion

Although the molecular nature of surface-adhesion receptors and their signaling cascades drive and control the process of adhesion, they are not individually the determinants of the dynamics of cell adhesion. Instead, our current studies show that the initial phases of cell spreading exhibit a general and conserved dynamical power-law behavior for the spreading radius, which is independent of the details of the underlying molecular interactions. This behavior is quantitatively consistent with a simple physical model based on the collective geometry and rheology of the cell and in particular that of the actin cortex, as parametrized by its thickness, viscosity, and adhesion-energy density. Taken together, our experiments and theory provide us with a unified framework for understanding the onset of cell spreading by focusing on the collective aspects of the cell whose behavior is determined by its coarse-grained geometry and material properties.

When viewed from a mesoscopic physicochemical perspective, this is perhaps not all that surprising given that the spreading rate is also a coarse-grained measurement that integrates many molecular details that occur on much smaller and faster scales. It is worth mentioning here that a variety of other molecular models

could lead to the same results. However, the constraints posed by experimental data are nontrivial (molecular nonspecificity and cortex geometry), suggesting that a macroscopic model that focuses on the collective material properties of the cell are sufficient to explain the data; they help us sharpen the question at the next level.

From a molecular biochemical perspective, our approach raises the question of the mechanisms and processes that determine the effective thickness of the cortex, perhaps the single most important determinant of the kinetics of spreading, because information about both the adhesion energy and the viscosity of the cortex comes naturally from knowledge of the geometry and constitutive structure of the cortex. Future attention on perturbing the molecular determinants of these material and geometric properties of cells in the context of their collective behavior will help us in carrying out an in-depth critical test of the proposed mechanism. A first step in this was uncovered by our experiments designed to disrupt the cortex. More refined experiments that quantify this disruption as well as others that probe the dynamics of the cortex directly will undoubtedly be needed to determine the molecular basis for the effective material parameters in our model. Although this will allow us to progress toward a hierarchical multiscale approach to the dynamics of cell spreading, simple quantitative laws and predictive physical models such as ours are an important step in providing guidance for future experiments.

Experimental Procedures

Cells and Substrates

HeLa (human adenocarcinoma epithelial cells) and S180 (mouse sarcoma cells) were cultured in DME (Dulbecco Modified Eagle) medium with 10% FCS (fetal-calf serum) at 37°C. Cells were treated with trypsin-calcium solution and centrifuged (1200 rpm, 5 min) for subsequent medium exchange. Prior to the experiments, cells were suspended in a working $C0_2$-independent medium (Invitrogen) devoid of FCS. S180 cells transiently transfected with a vector encoding for the constitutively inactive construct Cdc42DN were used for assessing the influence of the filopodial activity on the spreading dynamics. Red blood cells were obtained from finger prick and biotinylated with NHS-PEG3400-biotin (Nektar) [21]. When necessary, nocodazole (1 μM, 30 min) and cytochalasin D (1 μg/ml, 15 min) were added in working medium for disruption of, respectively, the microtubules and the actin filaments.

Glass coverslips were washed in chloroform/methanol:1/1 and used as templates for preparation of the substrates. Fibronectin coating was performed at 0.1 and 1 μg/ml in PBS for 30 min at 37°C. Polylysine was adsorbed from a 100 μg/ml solution at room temperature. E-cadherin was immobilized after a protocol adapted from [22]. In brief, coverslips were mercapto-silanized, loaded with goat anti-mouse Fcγ fragments antibodies (overnight, 20°C), and subsequently coated with human Ecad-Fc chimera (5 μg/ml, 4 hr, 37°C). Streptavidin was immobilized on a biotinylated coverslip [21] by incubation for 30 min at room temperature in a 10 μg/ml solution.

Video Microscopy and Analysis

The dynamics of cell spreading was followed by time-lapse reflection interference contrast microscopy (inverted Olympus IX 71 equipped with 100× apochromat objective, interference filter at 546 nm, and digital camera [Roper HQ]). Images were acquired every 1 or 5 s for approximately 30 min, and exposure times were 20 ms for eukaryotic cells. Real-time imaging at 50 Hz video rate was performed for erythrocytes. The (dark) contact area was measured from stacks of binary images with Metavue (Universal Imaging Corp.) in accordance with a standard threshold protocol [23]. Fixed cells [24] were visualized by 3D microscopy after plating for 30 min. Actin and DNA were stained with 1 μM phalloidin-FITC and DAPI. Vinculin was immunolabeled with primary anti-vinculin (kindly provided by Marina Glukhova) and secondary Cy3-conjugated goat anti-mouse antibodies. Image deconvolution was performed with the modified-Gold iterative constrained algorithm [25].

Supplemental Data

Supplemental Data include additional Discussion, four figures, one table, and eight movies and are available with this article online at http://www.current-biology.com/cgi/content/full/17/8/694/DC1/.

Acknowledgments

We thank Françoise Brochard-Wyart, Pierre-Gilles de Gennes, Jean-François Joanny, Patricia Bassereau, Elie Raphaël, David Quéré, David Mooney, and Manoj Chaudhury for many fruitful discussions. This work was supported by the Human Frontier Science Program through research grant #52/2003 to P.N. We also received generous help from the Institut Curie.

Received: October 10, 2006
Revised: February 20, 2007
Accepted: February 20, 2007
Published online: March 22, 2007

References

1. Zamir, E., and Geiger, B. (2001). Components of cell-matrix adhesions. J. Cell Sci. *114*, 3577–3579.
2. Balaban, N.Q., Schwarz, U.S., Riveline, D., Goichberg, P., Tzur, G., Sabanay, I., Mahalu, D., Safran, S., Bershadsky, A., Addadi, L., et al. (2001). Force and focal adhesion assembly: A close relationship studied using elastic micro-patterned substrates. Nat. Cell Biol. *3*, 466–472.
3. Dustin, M.L., Ferguson, L.M., Chan, P.Y., Springer, T.A., and Golan, D.E. (1996). Vizualization of CD2 interaction with LFA-3 and determination of the two-dimensional dissociation constant for adhesion receptors in a contact area. J. Cell Biol. *132*, 465–477.
4. Yauch, R.L., Felsenfeld, D.P., Kraeft, S.K., Chen, L.B., Sheetz, M.P., and Hemler, M.E. (1997). Mutational evidence for control of cell adhesion through integrin diffusion/clustering, independent of ligand binding. J. Exp. Med. *186*, 1347–1355.
5. Shenoy, V.B., and Freund, L.B. (2005). Growth and shape stability of a biological membrane adhesion complex in the diffusion-mediated regime. Proc. Natl. Acad. Sci. USA *102*, 3213–3218.
6. Chamaraux, F., Fache, S., Bruckert, F., and Fourcade, B. (2005). Kinetics of cell spreading. Phys. Rev. Lett. *94*, 158102.
7. Bereiter-Hahn, J., Lück, M., Miebach, T., Stelzer, H.K., and Vöth, M. (1990). Spreading of trypsinized cells: Cytoskeletal dynamics and energy requirements. J. Cell Sci. *96*, 171–188.
8. Cai, Y., Biais, N., Gianone, G., Tanase, M., Ladoux, B., Hofman, J., Wiggins, C.H., and Sheetz, M.P. (2006). Nonmuscle myosin IIA-dependent force inhibits cell spreading and drives F-actin flow. Biophys. J. *91*, 3907–3920.
9. Bruinsma, R., and Sackmann, E. (2001). Bioadhesion and the dewetting transition. Comptes Rendus de l'Academie des Sciences Series IV *2*, 803–815.
10. Dubin-Thaler, B.J., Giannone, G., Döbereiner, H.G., and Sheetz, M.P. (2004). Nanometer analysis of cell spreading on matrix-coated surfaces reveals two distinct cell states and STEPs. Biophys. J. *86*, 1794–1806.
11. Takeichi, M. (1991). Cadherin cell adhesion receptors as a morphogenetic regulator. Science *251*, 1451–1455.
12. Rohatgi, R., Ma, L., Miki, H., Lopez, M., Kirchhausen, T., Takenawa, T., and Kirschner, M.W. (1999). The interaction between N-WASP and the Arp2/3 complex links Cdc42-dependent signals to actin assembly. Cell *97*, 221–231.
13. Charras, G.T., Yarrow, J.C., Horton, M.A., Mahadevan, L., and Mitchison, T.J. (2005). Non-equilibration of hydrostatic pressure in blebbing cells. Nature *435*, 365–369.

14. Wottawah, F., Schinkinger, S., Lincoln, B., Ananthakrishnan, R., Romeyke, M., Guck, J., and Käs, J. (2005). Optical rheology of biological cells. Phys. Rev. Lett. *94*, 098103.
15. Lang, T., Wacker, I., Wunderlich, I., Rohrbach, A., Giese, G., Soldati, T., and Almers, W. (2000). Role of actin cortex in the subplasmalemmal transport of secretory granules in PC-12 cells. Biophys. J. *78*, 2863–2877.
16. Wang, N. (1998). Mechanical interactions among cytoskeletal filaments. Hypertension *32*, 162–165.
17. Heinrich, V., Ritchie, K., Mohandas, N., and Evans, E. (2001). Elastic thickness compressibility of the red cell membrane. Biophys. J. *81*, 1452–1463.
18. Markle, D.R., Evans, E.A., and Hochmuth, R.M. (1983). Force relaxation and permanent deformation of erythrocyte membrane. Biophys. J. *42*, 91–98.
19. Pierrat, S., Brochard-Wyart, F., and Nassoy, P. (2004). Enforced detachment of red blood cells adhering to surfaces: Statics and dynamics. Biophys. J. *87*, 2855–2869.
20. Hategan, A., Sengupta, K., Kahn, S., Sackmann, E., and Discher, D.E. (2004). Topographical pattern dynamics in passive adhesion of cell membranes. Biophys. J. *87*, 3547–3560.
21. Merkel, R., Nassoy, P., Leung, A., Ritchie, K., and Evans, E. (1999). Energy landscapes of receptor-ligand bonds explored with dynamic force spectroscopy. Nature *397*, 50–53.
22. Lambert, M., Padilla, F., and Mège, R.M. (2000). Immobilized dimers of N-cadherin-Fc chimera mimic cadherin-mediated cell contact formation: Contribution of both outside-in and inside-out signals. J. Cell Sci. *113*, 2207–2219.
23. Pierres, A.P., Eymeric, P., Baloche, E., Touchad, D., Benoliel, A.M., and Bongrand, P. (2003). Cell membrane alignment along adhesive surfaces: Contribution of active and passive cell processes. Biophys. J. *84*, 2058–2070.
24. Mitchison, T.J. (1992). Actin based motility on retraction fibers in mitotic PtK2 cells. Cell Motil. Cytoskeleton *22*, 135–151.
25. Sibarita, J.B. (2005). Deconvolution Microscopy. Adv. Biochem. Eng. Biotechnol. *95*, 201–243.

Supplemental Data

The Universal Dynamics of Cell Spreading

Damien Cuvelier, Manuel Théry, Yeh-Shiu Chu, Sylvie Dufour, Jean-Paul Thiéry, Michel Bornens, Pierre Nassoy, and L. Mahadevan

Supplemental Discussion

Theoretical Model: Assumptions and Implications

Our basic starting point is the geometry of the spreading cell, which we model as a polymeric viscous shell (the cortex-bilayer composite) surrounding a less viscous interior, the cytoplasm.

We also assume that the viscosity of the aqueous environment of the cell is much smaller than that of the cell, so that we do not have to consider its effects as rate limiting over the period of observations. Further, we assume that although energy is continuously consumed by the cell, it is not in the main directed toward the active protrusion of lamellipodia, cell polarization, etc.

Because we see that the same power law results from a variety of cell types adhering to different substrates with varying concentrations of ligands, we assume that the dynamics of adhesion is not determined by specific chemical interactions to leading order. This is reasonable when one thinks about the situation in detail: Although at the molecular level, receptor-ligand interactions are indeed important, the time scales for these are relatively short and of the order of a few ms. However, the adhesive contact changes because of the relatively slow

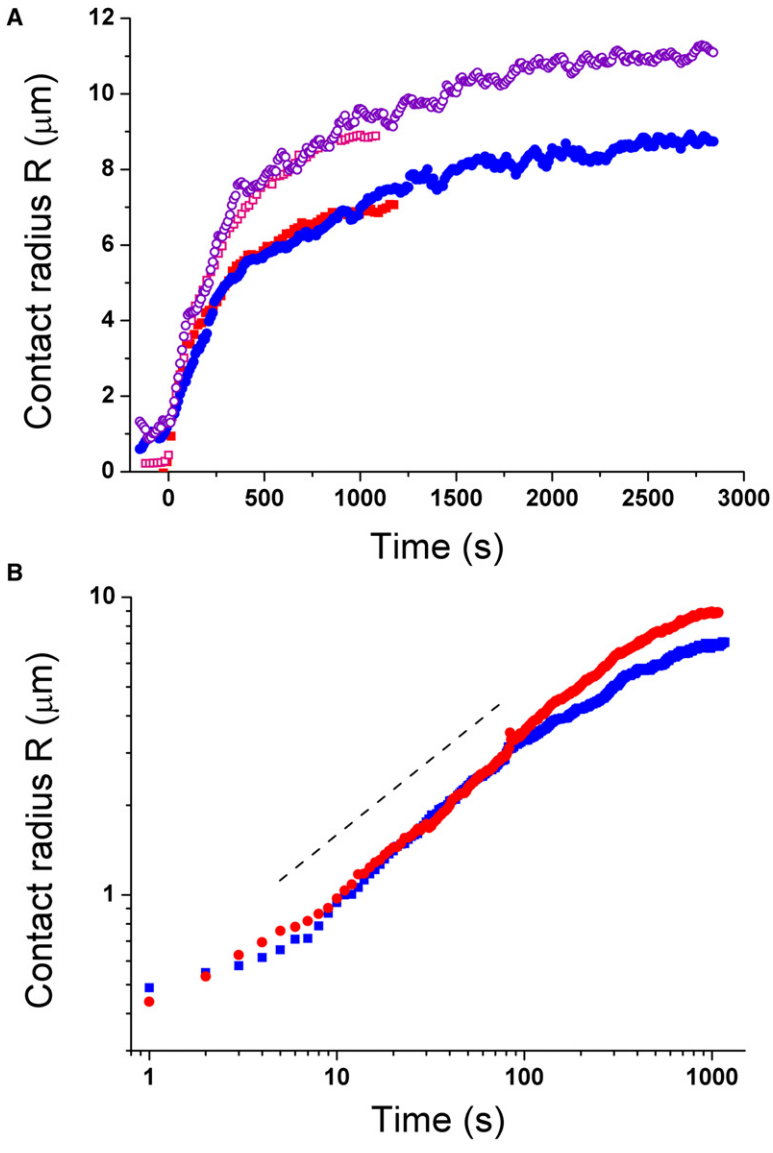

Figure S1. Influence of the Surface Density in Fibronectin and of the Cell Line on the Spreading Dynamics

(A) Time evolutions of the contact radius for two cell lines and two different concentrations of fibronectin are as follows: blue closed circles, S180 cell/fibronectin (0.1 μg/ml); purple open circles, S180 cell/fibronectin (1 μg/ml); red closed squares, HeLa cell/fibronectin (0.1 μg/ml); and magenta open squares: HeLa cell/fibronectin (1 μg/ml).

(B) Time evolution of the contact radius of a HeLa cell sreading onto a fibronectin-coated substrate (blue: 0.1 μg/ml; red: 1 μg/ml) in a log-log plot. The dashed line is a guide indicating the power law $t^{1/2}$.

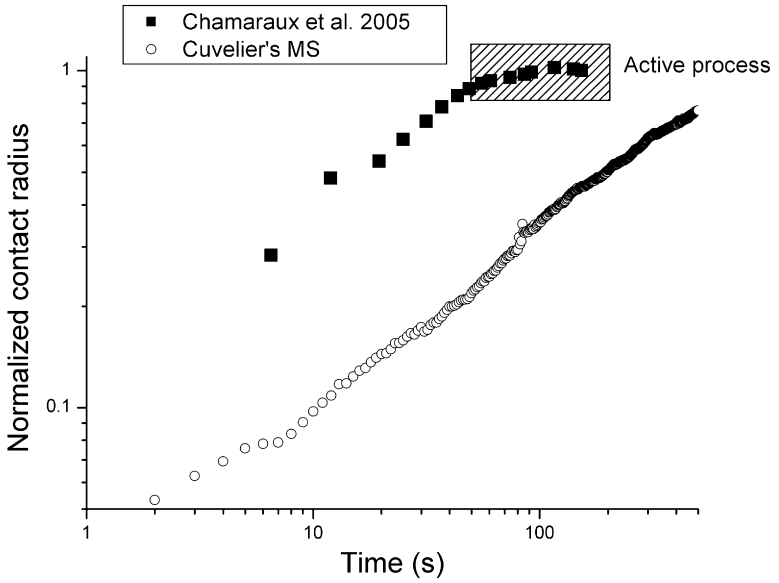

Figure S2. Contact Radius versus Time for *Dictyostelium discoideum* Spreading on Bare Glass

Data from Chamaraux et al. [S1] are replotted in a log-log scale and compared with one typical curve of the present work.

flow, occurring over a time scale of many seconds, of the dense entangled and crosslinked cortex. This separation of time scales implies that a simple physicochemical interfacial adhesive energy density suffices to describe the process: Characterizing this requires the specification of the energy of interaction of a single receptor-ligand bond and the areal density of bonds, which we assume is limited by the density of ligands on the substrate rather than the number of receptors that the cell is capable of supplying. This is reasonable for live cells but must be contrasted sharply with the assumption made in studies of vesicle adhesion, where, for example, the membrane-based diffusion of receptors is often the rate-limiting step. If J is the adhesion energy density (in J/m^2) of the cell, the change in adhesion energy when the contact line of radius R and length $2\pi R$ moves an amount dR is given by $2\pi RdR$; if this occurs in a time dt, the rate of change of energy associated with adhesion is proportional to $JR\frac{dR}{dt}$ (here and elsewhere, we will ignore numerical factors such 2 π because our goal is to uncover the basic functional dependences).

The dynamics of adhesion is limited by the resistance to flow of the cell as a whole as it spreads from a spherical shape to a flattened one. With the exception of the nucleus, the cortex is by far the densest part of the cell. Because the cortex must flow to accommodate the excess area associated with spreading (whereas the nucleus does not), the rate of flattening is determined by the time required for the cortex to deform. The cortex is elastic at short times and viscous at long times; in general its rheology, i.e., its response to forces, is complex. During the slow irreversible spreading of the cell, we assume that the viscous flow of the cortical layer provides the dominant resistance to the rate of deformation; furthermore, we assume that the cortex behaves like a simple Newtonian viscous liquid, i.e., its viscosity $\eta$is constant. The rate of dissipation in a fluid is proportional to $\int \eta(\nabla u)^2 dv$ where ∇u is the velocity gradient or shear rate in the dense entangled cortex. Assuming

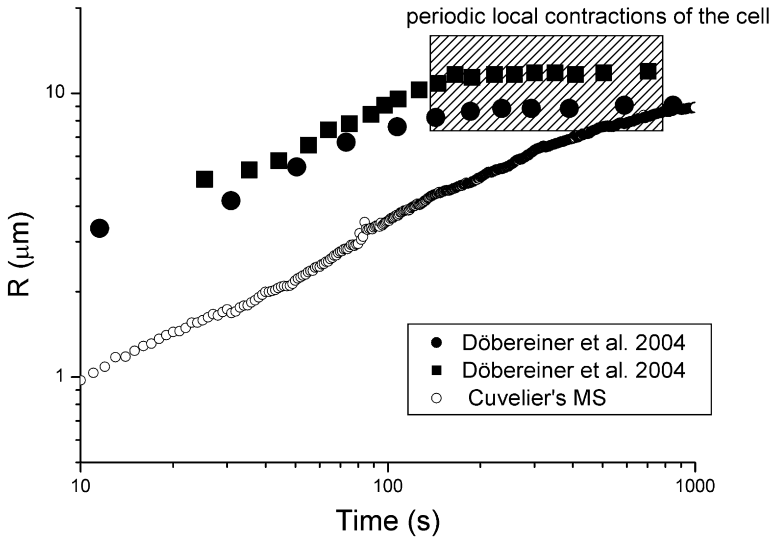

Figure S3. Contact Radius versus Time for Fibroblast Spreading on Fibronectin-Coated Glass

Data from Dubin-Thaler et al. [S6] are replotted in a log-log scale and compared with one typical curve of the present work.

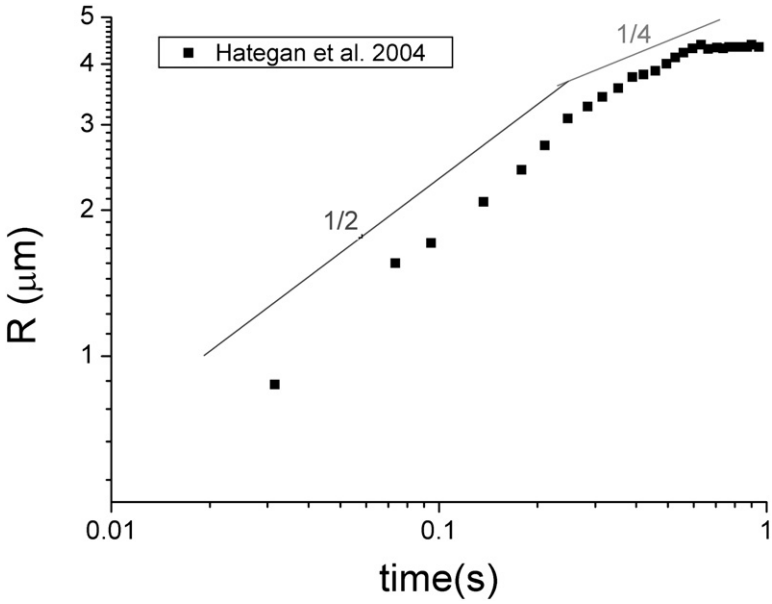

Figure S4. Contact Radius versus Time for Red Blood Cell Spreading on Polylysine-Coated Glass

Data from Hategan et al. [S8] are replotted in a log-log plot. The lines are guide lines showing the growth law for the two regimes discussed in the present paper.

that the velocity varies from zero at the adhesive interface between the cell and the substrate to the velocity of the contact line dR/dt at the innermost layer of the cortex of thickness w, a typical velocity gradient in this zone is $\nabla u \sim 1/w(dR/dt)$. Here, we have made the assumption that the velocity of unbending the cortex in the vicinity of the contact line dR/dt is the velocity at which the cortex is sheared. For situations when the size of the contact zone is comparable to the entanglement of the filaments in cortex, the volume affected by the shearing is proportional to $\int dv \sim R^2 w$, i.e., it is the area of the contact zone multiplied by the cortical thickness. Substituting these expressions into the dissipation rate is proportional to $\eta(\frac{dR}{wdt})^2 R^2 w$. Balancing this dissipation rate with the adhesive power yields the scaling law (Equation 1).

Similar arguments, but with different expressions for the shear rate and the volume over which the dissipation occurs, under conditions corresponding to a flattened cell lead to the scaling law (Equation 2) and the linear behavior observed for cell spreading without a cortex.

Having outlined the assumptions and implications of the mesoscopic theory, we can clearly see its strengths and limitations. The main strength of the model is its relative simplicity and the fact that it can with minor modifications explain a variety of different scenarios of spreading. When combined with complementary models in the limit of diffusion-limited spreading in vesicles, we find that the range of phenomena that may be explained includes vesicle and cell spreading; also, the model could be used to look at phenomena such as phagocytosis and endocytosis. Furthermore, the parameters that the model requires are all measurable quantities, and its predictions are consistent with observations for the diffusive spreading of the cell at short and intermediate times. A key prediction is that destroying the cortex should alter the dynamics of spreading qualitatively; experimentally we see subdiffusive spreading in this situation. The main limitation of the model is that it assumes a constant cortical thickness and viscosity, both of which have molecular determinants that are not yet completely known.

Table S1. Summary of Experimental Conditions and Fitting Parameters

Cell Type	Surface Coating (concentration[a])	Number of Cells	Exponent α[b] ($R \sim t^{\alpha}$)	Adhesion Energy[b] J ($\mu J/m^2$)
HeLa/S180	Fibronectin (1 μg/ml)	18	0.51 ± 0.03	40 ± 16
HeLa/S180	Fibronectin (0.1 μg/ml)	16	0.47 ± 0.05	8 ± 3
HeLa	Polylysine (100 μg/ml)	9	0.50 ± 0.04	138 ± 22
S180-Ecad	E-Cadherin (5 μg/ml)	12	0.48 ± 0.02	31 ± 7
Cdc42DN-S180	Fibronectin (1 μg/ml)	7	0.49 ± 0.03	75 ± 31
Nocodazol-treated HeLa	Fibronectin (10 μg/ml)	9	0.45 ± 0.07	101 ± 42
Biotinylated Erythrocyte	Streptavidin (10 μg/ml)	19	0.50 ± 0.02	88 ± 7
Cytochalasin-treated HeLa	Fibronectin (1 μg/ml)	13	0.95 ± 0.06	30 ± 8[c]

Note that the fits are performed from the onset of spreading to a radius of contact equal to the cell radius (i.e., 7 μm for eukaryotic cells and 3 μm for erythrocytes).

[a] Bulk concentration used to coat the glass slides (see Experimental Procedures for protocol details).

[b] Experimental data were fitted with two parameters, α and J. The unknown constant in Equation 1 was chosen as C = 2. For HeLa and S180 cells, the cortex thickness was set at w = 1 μm [S12], and the effective viscosity of the cortex η = 300 Pa.s [S13]. For erythrocytes, w = 50 nm [S10] and η=10 Pa.s [S11].

[c] The interior viscosity of cytochalasin D-treated cells was set = 150 Pa.s.

Quantitative Interpretation of Previous Experimental Results in the Framework of Our Theoretical Model

Here, we use the quantitative framework developed by us to analyze earlier experiments that report data on the early stages of cell spreading with sufficient precision that allows for analysis. In these works, the selected cells and adhesive surfaces are strikingly different, and yet they show the same quantitative trends as we see. For each case, we have extracted the original data and plotted the R-t curve in log-log plot together with one of our typical curves. We have then attempted to account for the observed kinetics on the basis of our three-parameter model (viscosity η, adhesion-energy density J, and cortex thickness w).

(1) Spreading of *Dictyostelium discoideum* on Bare Glass [S1]

As pointed out by the authors, the growth of the contact area is intrinsically directional with *D. discoideum* (even at short times), with an immobile backfront. The model proposed by Chamaraux et al. suggests that the spreading dynamics is primarily governed by the kinetics of actin polymerization. This assumption seems reasonable given the polarized nature of *D. discoideum*. In consequence, six independent microscopic parameters that may be difficult to measure are required to account for the observed growth law. The authors propose that the contact area is proportional to $\tanh(\alpha t)$, with α^{-1} being a characteristic time, of the order of 50 s.

For $t < 50$ s, the contact area increases linearly with time. The average contact radius thus is proportional to $t^{1/2}$ before saturating at longer times (>1 min), for which active processes strongly dominate the dynamics of spreading and motility.

As seen in Figure S2, the agreement between this approximate power law and the one predicted by our model might be coincidental. However, by taking $A = 100\ \mu m^2$ for the "equilibrium contact area" (see for instance [S2]), the spreading rate at short times is of the order of $1.5\ \mu m^2/s$. With $w = 1\ \mu m$ and $J = 20\ \mu J/m^2$ [S3], we find a cortex viscosity of the order of 50 Pa.s for *D. discoideum*, and this is in good agreement with the 10–250 Pa.s range reported in [S4].

(2) Spreading of Fibroblasts on Fibronectin-Coated Glass Surfaces in Serum-Free Medium [S5, S6]

The authors report three regimes of growth for the adhesive patch characterized by three power laws. The derived exponents are, respectively, 0.4 ± 0.2, 1.6 ± 0.9, and 0.3 ± 0.2 for the contact area. First, we may note that the amount of error on these exponents is very large. Second, when displayed as R versus t in a log-log plot, we observe that these three power laws are obtained over half a decade in radius (y axis) and less than two decades in time (x axis). We propose that their data could be reinterpreted by considering that the first stage is a quiescent stage preceding the effective spreading of the cell. Subtracting this lag time, we find that their intermediate regime is astonishingly well described by a $t^{1/2}$ law (see Figure S3). The global shift toward large patch sizes for a given time may also be rationalized by the lower cortex viscosity of fibroblasts compared to most other cells [S7]. Finally, at later stages (corresponding to the third regime), the contact radius seems to saturate instead of growing proportional to $t^{1/4}$. As pointed out in our manuscript, this $t^{1/4}$ regime may be overwhelmed by active processes because this seems to occur in this particular case (the authors report "periodic local contractions of the cell") and is clearly outside the range of applicability of our model.

(3) Spreading of Red Blood Cells on Polylysine-Coated Glass [S8]

The authors have monitored the spreading kinetics of a red blood cell onto a polylysine-coated (10 mg/ml bulk concentration) substrate. Here, the kinetics is completed within 1 s, which is three orders-of-magnitude more quickly than for HeLa cells on ECM substrates, for example. In this particular case, however, all the parameters η, J, and w were measured by independent methods. In a previous paper, Hategan et al. [S9] determined that the adhesion energy (referred to as "spreading pressure") is $J \approx 10^{-3}\ J/m^2$. From thickness measurement of the erythrocyte sprectrin network, Heinrich et al. [S10] found that w = 50 nm. Finally, shape-relaxation measurements of deformed red blood cells yielded a cortex viscosity $\eta = 10$ Pa.s [S11]. From Equation 1 (see main text), one readily obtains $dA/dt = 60\ \mu m^2/s$, and the measured growth rate was found to be $123\ \mu m^2/s$. Given the uncertainty on the measured parameters and on the prefactor in Equation 1, a difference by a factor 2 has to be considered as a good agreement.

The R-versus-t curve also displays a break in the slope. The log-log plot shown in Figure S4 could suggest a $t^{1/4}$ power law. If one fits this portion of curve with Equation 2, we find $(JR_c^3/\eta)^{1/4} = 4$, whereas the calculated value of the prefactor with the measured values of J, η, and R_c yields 7. Recognizing that Equation 2 is a scaling law, in which a small numerical factor has been omitted, the reported data is consistent with our model for both regimes.

Supplemental References

S1. Chamaraux, F., Fache, S., Bruckert, F., and Fourcade, B. (2005). Kinetics of cell spreading. Phys. Rev. Lett. *94*, 158102.

S2. Decave, E., Rieu, D., Dalous, J., Fache, S., Brechet, Y., Fourcade, B., Satre, M., and Bruckert, F. (2003). Shear flow-induced motility of Dictyostelium discoideum cells on solid substrate. J. Cell Sci. *116*, 4331–4343.

S3. Simson, R., Wallraff, E., Faix, J., Niewoehner, J., Gerisch, G., and Sackmann, E. (1998). Membrane bending modulus and adhesion energy of wild-type and mutant cells of Dictyostelium lacking talin or cortexillins. Biophys. J. *74*, 514–522.

S4. Feneberg, W., Westphal, M., and Sackmann, E. (2001). Dictyostelium cells' cytoplasm as an active viscoplastic body. Eur. Biophys. J. *30*, 284–294.

S5. Dobereiner, H.G., Dubin-Thaler, B., Giannone, G., Xenias, H.S., and Sheetz, M.P. (2004). Dynamic phase transitions in cell spreading. Phys. Rev. Lett. *93*, 108105.

S6. Dubin-Thaler, B.J., Giannone, G., Döbereiner, H.G., and Sheetz, M.P. (2004). Nanometer analysis of cell spreading on matrix-coated surfaces reveals two distinct cell states and STEPs. Biophys. J. *86*, 1794–1806.

S7. Karcher, H., Lammerding, J., Huang, H., Lee, R.T., Kamm, R.D., and Kaazempur-Mofrad, M.R. (2003). A three-dimensional viscoelastic model for cell deformation with experimental verification. Biophys. J. *85*, 3336–3349.

S8. Hategan, A., Sengupta, K., Kahn, S., Sackmann, E., and Discher, D.E. (2004). Topographical pattern dynamics in passive adhesion of cell membranes. Biophys. J. *87*, 3547–3560.
S9. Hategan, A., Law, R., Kahn, S., and Discher, D.E. (2003). Adhesively-tensed cell membranes: Lysis kinetics and atomic force microscopy probing. Biophys. J. *85*, 2746–2759.
S10. Heinrich, V., Ritchie, K., Mohandas, N., and Evans, E. (2001). Elastic thickness compressibility of the red cell membrane. Biophys. J. *81*, 1452–1463.
S11. Markle, D.R., Evans, E.A., and Hochmuth, R.M. (1983). Force relaxation and permanent deformation of erythrocyte membrane. Biophys. J. *42*, 91–98.
S12. Lang, T., Wacker, I., Wunderlich, I., Rohrbach, A., Giese, G., Soldati, T., and Almers, W. (2000). Role of actin cortex in the subplasmalemmal transport of secretory granules in PC-12 cells. Biophys. J. *78*, 2863–2877.
S13. Wang, N. (1998). Mechanical interactions among cytoskeletal filaments. Hypertension *32*, 162–165.